Comparing Orientation-Dependent Transverse Relaxation at 3T and 7T: Deciphering Anisotropic Relaxation Mechanisms in White Matter

Yuxi Pang, Rajikha Raja, and Wilburn E. Reddick

Department of Radiology,

St. Jude Children's Research Hospital, Memphis, TN, USA

Corresponding Author:

Yuxi Pang, PhD

Department of Radiology

St. Jude Children's Research Hospital

262 Danny Thomas Place, MS 220

Memphis, TN, 38105-3678 USA

Email: yuxi.pang@stjude.org

ORCID ID: https://orcid.org/0000-0001-5039-0236

Running Title: Comparing Orientation-Dependent Transverse Relaxation at 3T and 7T

Word Count: 5139

Keywords: *diffusion tensor imaging, human brain white matter, magic angle effect, magnetic susceptibility, orientation-dependent transverse relaxation mechanism.*

Abbreviations: *AR, angular resolution; CC, corpus callosum; CG, cingulum; CNS, central nervous system; DTI, diffusion tensor imaging; FA, fractional anisotropy; HCFM, hollow cylinder fiber model; HCP, Human Connectome Project; NP, number of points; MAE, magic angle effect; MO, mode of anisotropy; ODF, orientation distribution function; PNS, peripheral nervous system; RDI, residual dipolar interaction; SAR, specific absorption rate; T2W, T_2-weighted; WM, white matter.*

ABSTRACT

Purpose: This work aims to elucidate the mechanisms underlying orientation-dependent transverse relaxation in human brain white matter (WM), which have long been ambiguous.

Methods: We analyzed publicly available 3T and 7T DTI datasets (*b*-values = 1000 and 2000 s/mm^2) from 25 young adults participating in the Human Connectome Project. Orientation-dependent transverse relaxation R_2 profiles from whole brain WM were generated from T_2-weighted images (*b*-value = 0) and characterized using a previously developed cone model based on the generalized magic angle effect (MAE). Derived anisotropic R_2 or R_2^a values were compared between different magnetic fields. Similar comparisons were also conducted for the derived R_2^a values from whole brain WM and two fiber tracts, based on gradient-echo signals reported in the literature. Classical relaxation theories predict that the ratio of $R_2^a(7T)/R_2^a(3T)$ will be unity or $(7/3)^2$ (i.e., approximately 5.4) if the measured orientation-dependent R_2 arises exclusively from MAE or from the previously proposed susceptibility effect, respectively.

Results: Fitted model parameters were comparable for DTI datasets with *b*-values of 1000 and 2000 (s/mm^2). The fitted R_2^a increased, on average, from 3.6±1.1 (1/s) at 3T to 5.4±1.5 (1/s) at 7T for DTI datasets with a *b*-value=1000 s/mm^2. The measured ratio of $R_2^a(7T)/R_2^a(3T)$ was thus approximately 1.5. However, based on gradient-echo signals, this ratio essentially became unity within the measurement precision.

Conclusion: This study suggests that MAE is the primary mechanism for the observed orientation-dependent transverse relaxation at 3T in human brain WM, offering a different perspective from previous literature.

1 | INTRODUCTION

The distinct contrasts observed in magnetic resonance (MR) imaging of biological tissues are significantly influenced by the composition of biomolecular constituents and their hierarchical organization.[1,2] Approximately two decades ago, the increasing availability of whole-body MR scanners operating at ultra-high magnetic B_0 fields led to the discovery of unprecedented varying T_2^* contrast in the gradient-echo images of human brain white matter (WM) in vivo at 7T.[3,4] This characteristic T_2^* contrast, or its reciprocal R_2^* contrast, was found to depend on the orientation of axon fiber tracts in a subsequent animal study,[5] where the anesthetized animal brain was orientated in different positions. Shortly thereafter, a clearer picture emerged from another study performed on healthy human brains at 3T,[6] where the R_2^* values from the fiber tracts were found to be larger along either left-right or anterior-posterior direction than along the inferior-superior direction or the direction of the B_0 field. Moreover, the observed R_2^* values appeared proportionally correlated with diffusion fractional anisotropy (FA) derived from diffusion tensor imaging (DTI).

The actual profiles of R_2^* orientation dependences of human brain WM in vivo at 3 T were eventually established by exploiting orientation information from DTI via the principal diffusivity (λ_1) direction within an imaging voxel.[7,8] More importantly, an orientation-dependent function of $\sin^2\theta$ or $\sin 2\theta$ was proposed, where θ is the angle formed between the directions of λ_1 and B_0. In a subsequent study of two coronal formalin-fixed brain slabs at 7T,[9] an improved orientation-dependent function was developed, incorporating an additional term of $\sin 4\theta$. This improved function was determined based on the R_2^* measurements of brain specimens rotating at 18 different angles around the brain slab's norm direction, spanning from 0° to 170° with respect to the direction of the B_0 field. In this ex vivo study, the investigators introduced the concept of

phase-shift φ_0 into the proposed R_2^* orientation-dependent function. However, the biophysical basis of φ_0 was not adequately elucidated. As a result, this phase-shift was often omitted when applying the proposed function to previously reported studies, where orientation information was derived from λ_1 in DTI.[10-12]

To better understand the origins of the observed orientation-dependent transverse relaxation in WM, a further investigation was conducted at 7T on rotating brain specimens, following a similar workflow as mentioned above.[13] In this comparative study, unlike the observed R_2^* anisotropy, the measured R_2 hardly exhibited any discernible anisotropy. This observation led the investigators to believe that the susceptibility effect was the dominant anisotropic relaxation mechanism. However, the temperature-dependent anisotropies of R_2^* from the brain samples could not be adequately explained with the proposed relaxation mechanism. These conflicting findings clearly illustrate that the actual origin of orientation-dependent R_2^* in WM remains elusive.

Meanwhile, researchers developed a hollow cylinder fiber model (HCFM) in WM based on susceptibility theory.[14,15] In this model, the annular region of the cylinder was filled with molecular constituents exhibiting anisotropic magnetic susceptibilities, predicting the R_2^* orientation dependence with an analytical function that includes a term of $\sin^4\theta$ or $\sin 4\theta$.[14] However, this analytical function was insufficient for characterizing the shape of orientation-dependent R_2^* profiles derived from rotating pig brain samples unless it included an additional heuristic term of $\sin^2\theta$. Interestingly, a similar orientation-dependent R_2 function, incorporating the term $\sin^4\theta$, with and without the term $\sin^2\theta$, was also proposed for human brain WM in vivo at 3T.[16] The underlying physical principle of the proposed model for R_2 anisotropy was the same susceptibility theory for R_2^* anisotropy but applied on a mesoscopic scale.

The well-known magic angle effect (MAE),[17] related to rotationally restricted water molecules in highly ordered biological tissues,[18] has been inadequately considered in the developed orientation-dependent R_2^* or R_2 relaxation theories.[9,19] This oversight is partially due to the drastically different profiles of the measured R_2^* or R_2 orientation dependences in WM, where an enhanced relaxation rate is observed for axon fibers orientated perpendicular to B_0 compared to parallel.[6] In contrast, conventional MAE profiles, such as those found in tendons and deep-zone cartilage, show the opposite relaxation rate enhancement between the two axon fiber orientations.[17] Recently, this seemingly contradictory R_2^* or R_2 anisotropy in WM has been resolved by employing a generalized MAE function incorporating a phase shift.[20,21] Remarkably, this proposed MAE-based function can be expressed in the forms of previously developed orientation-dependent R_2^* and R_2 functions, thus revealing an ambiguous mechanism governing anisotropic transverse relaxation in WM as previously reported in the literature.[13,22]

Orientation-dependent transverse relaxation is directly related to the extent of (de)myelination in WM, providing unprecedented specificity in neuro microstructural imaging.[13,15,21,23] To accurately represent the underlying biophysical processes, it is essential to separate the previously proposed relaxation mechanisms — namely, the susceptibility effect and MAE — for R_2^* and R_2 anisotropies. This separation will enhance our understanding of the unique relaxometries related to the highly organized microstructures in WM. Given the current ambiguity surrounding the mechanism of anisotropic transverse relaxation, this work aims to elucidate the long-standing equivocal origins of orientation-dependent transverse relaxation in human brain WM.

2 | THEORY

This section provides a brief overview of previously developed biophysical models for orientation-dependent R_2^* and R_2 in brain WM. The literature demonstrates that the orientation dependence of R_2^*, equivalent to R_2+ R_2', originates from R_2 rather than R_2'.[14] It was believed that R_2' is primarily due to non-local effects stemming from large length-scale B_0 inhomogeneities and macroscopic variations in magnetic susceptibility. Consequently, R_2^* and R_2 are treated interchangeably in this study when considering their orientation dependences,[20] despite being derived from multiple gradient-echo and multiple spin-echo datasets, respectively.

2.1 | Susceptibility-based models for R_2^* and R_2 orientation dependences

According to the previously proposed HCFM model,[14,15] an orientation-dependent function for R_2^* is given in Equation 1, which includes an analytically derived term $\sin^4\theta$ and a heuristic term $\sin^2\theta$. The latter term is essential to account for myelin water contributions to the simulated and observed R_2^* values in WM.[14] A seemingly different but mathematically equivalent orientation-dependent function for R_2^* is also developed in the literature,[13] as expressed in Equation 2.

$$R_2^* = A_0 + A_1 \sin^2\theta + A_2 \sin^4\theta \qquad [1]$$

$$R_2^* = B_0 + B_1 \cos 2\theta + B_2 \cos 4\theta \qquad [2]$$

Although mathematically equivalent,[22] these two functions were developed from two drastically different biophysical underpinnings. In deriving Equation 2, a so-called inhomogeneous broadening or static dephasing was assumed,[24] where the terms $\cos 2\theta$ and $\cos 4\theta$ were respectively attributed to the highly ordered myelin microstructures and the corresponding susceptibility anisotropies.[13] In contrast, the terms $\sin^2\theta$ and $\sin^4\theta$ in Equation 1 originated from the assumed inhomogeneous broadening effect for myelin waters and the homogeneous broadening effect for intra- and extra-axonal waters, respectively.[14]

Interestingly, Equation 1 was also proposed for characterizing R_2 orientation dependences,[16] in which the $\sin^4\theta$ term stems from diffusion-mediated decoherence due to magnetic susceptibility differences on the mesoscopic scale, and the $\sin^2\theta$ term is caused by the interaction between susceptibility differences and applied field gradients. Obviously, the latter contribution should be insignificant within standard spin-echo datasets. Nevertheless, this $\sin^2\theta$ term appeared to be inevitable to better fit orientation-dependent R_2 profiles in WM.[12,22]

2.2 | A unified model based on MAE

Given the self-conflicting biophysical bases underlying previously developed models, a unified function has been proposed that solely depends on the well-known MAE in WM.[20,21] As schematically shown in Figure 1A, adapted from the literature,[25] a typical myelinated axon fiber is wrapped by multiple layers of bilayer membranes. Rotationally restricted water can concurrently reside in an axonal space,[10,26] denoted by a filled violet circle, and in the spaces accommodating myelin water,[27] signified by the word H2O (Figure 1B). For the latter case, the proton-proton (H-H) residual dipolar interaction (RDI) vectors from rotationally restricted water are assumed to lie within the plane that cuts perpendicularly through the axon fiber (Figures 1A-C).[21] In contrast, the RDI vectors within the axonal space are assumed to align with the axial direction of the axon fiber.[10]

A unified function was derived by evaluating the effective RDI vectors within an axially symmetric system or a cone model (Figure 1E) with an open angle α that represents relative contributions from within (α = 0°) and outside (α = 90°) an axon fiber (Figure 1D).[21] In this model, individual vectors, characterized by an orientation-dependent function $(3\cos^2\theta - 1)^2$, align along the wall of the cone. If the cone's axially symmetric axis makes an angle ε to the B_0

direction, the orientation dependence of R_2 from this ensemble of RDI vectors can be concisely expressed by Equation 3.[20,21]

$$f(\alpha,\varepsilon) = \frac{1}{4}(3\cos^2\alpha - 1)^2(3\cos^2\varepsilon - 1)^2 + \frac{9}{8}(\sin^4\alpha\,\sin^4\varepsilon + \sin^2 2\alpha\,\sin^2 2\varepsilon) \qquad (3)$$

It has been shown before that Equations 1-3 are equivalent.[20,22] When the condition $\alpha = 0°$ is met, the derived general orientation-dependent function will be restored to the conventional MAE function, i.e., $f(0°,\varepsilon) = (3\cos^2\varepsilon - 1)^2$. On the other hand, if α changes to 90°, $f(90°,\varepsilon)$ becomes $(1/4)(3\cos^2\varepsilon - 1)^2 + (9/8)(\sin^4\varepsilon)$. As shown in Figure 1F, the orientation-dependent profile (black) of $f(0°,\varepsilon)$ markedly differs from that (blue) of $f(90°,\varepsilon)$.

The measured transverse relaxation R_2 in WM could be commonly divided into an orientation-independent R_2^i part and a counterpart of the orientation-dependent $R_2^a(\alpha,\varepsilon)$ or $R_2^a \times f(\alpha,\varepsilon)$, as shown in Equation 4. For the case of R_2^*, i.e., $R_2 + R_2'$, R_2' has been folded into R_2^i. It is worth mentioning that R_2^i is always assumed to be constant when considering an orientation-dependent phenomenon of the measured R_2 in biological tissues.

$$R_2 = R_2^i + R_2^a \times f(\alpha,\varepsilon) \qquad (4)$$

2.3 | B_0-dependence of anisotropic transverse relaxation rates

As shown above, Equations 1-3 are mathematically equivalent yet derived from different biophysical bases. Therefore, it is impossible to separate different relaxation mechanisms, i.e., the susceptibility effect and MAE, merely by rearranging some orientation-dependent terms in the previously proposed model functions.[13,22] If the susceptibility mechanism were the only pathway for orientation-dependent relaxation, R_2^a should be proportional to B_0^2.[14] On the other hand, R_2^a would become completely independent of B_0 when MAE is responsible for anisotropic transverse relaxation.[28]

Accordingly, the different relaxation mechanisms can be disentangled by comparing R_2^a derived from two different magnetic B_0 fields, as shown in the literature.[29] For instance, the ratio, denoted by η, between the two R_2^a values measured at 7T and 3T is theoretically predicted as $\eta = (7/3)^2$ or 5.44, assuming the increase in R_2^a from 3T to 7T is solely due to the susceptibility effect. When considering the actual B_0 field strengths of 2.895T and 6.980T used in data acquisitions,[30] η increases slightly from 5.44 to 5.81. This more realistic η value will be used for the following data analysis in this work; however, the actual field strengths will still be referred to as 3T and 7T throughout the text for convenience.

In a different scenario, the susceptibility effect could be partially responsible for the observed R_2^a in WM. In this case, the extent to which this specific effect contributes to the measured R_2^a at 3T can be quantified as $100*\Delta R_2^a/(R_2^a(3T) * \eta)$ in terms of percentage, where ΔR_2^a denotes the increase in R_2^a measured from 3T to 7T, i.e., $\Delta R_2^a = R_2^a(7T) - R_2^a(3T)$. A convincing conclusion regarding the relative importance of the specific anisotropic transverse relaxation mechanism should remain consistent, regardless of whether R_2^a is measured using the gradient-echo or spin-echo signals.

3 | METHODS

3.1 | DTI datasets at 3T and 7T from HCP

We randomly selected 25 subjects from 184 young adults in the Human Connectome Project (HCP) (https://www.humanconnectome.org/study/hcp-young-adult), who had diffusion tensor imaging (DTI) datasets acquired at 3T with a spin-echo time (TE) = 89 ms, as well as at 7T with a TE = 71 ms. As shown in Tables 1 and 2, each subject was identified by Subject Number (1st column) used in this study, in addition to HCP-ID (2nd column) that specified the subject's

original HCP identification number, gender, and age. For instance, the 15th subject's original HCP identification number was 385046, the gender was male (M), and the age was 28 years.

These DTI datasets had been preprocessed to correct image artifacts arising from signal drifts, susceptibilities, eddy currents, gradient nonlinearity-induced distortions, and participant involuntary head motions. Data subsets with *b*-values = 0, 1000 (s/mm^2) and *b*-values = 0, 2000 (s/mm^2) were separately fitted using FSL DTIFIT software.[31] The fitted parameters included three eigenvalues (λ_1, λ_2, λ_3), three eigenvectors ($\hat{e}_1$, $\hat{e}_2$, $\hat{e}_3$), FA (fractional anisotropy), MO (mode of anisotropy),[32] and T_2-weighted (T2W) images. The direction (Φ) of the principal diffusivity λ_1, with respect to the B_0 direction, was represented by the primary eigenvector $\hat{e}_1$ via the relationship: $\cos\Phi = \hat{e}_1.B_0/\|\hat{e}_1.B_0\|$.[7,12]

As shown in the literature,[20,21] R_2^a can be extracted from T2W images provided voxel-wise fiber orientations (ε). Typically, a typical voxel signal from the T2W image, $S_{b=0}$, can be expressed using Equation 5:

$$S_{b=0} = M_0 exp\left(-\left(R_2^i + R_2^a \times f(\alpha,\varepsilon)\right)TE\right). \qquad (5)$$

Herein, M_0 is the maximum signal amplitude when TE reduces to zero. In a logarithmic scale, Equation 5 can be recast into Equation 6:

$$\ln S_{b=0}/TE = C_0 - R_2^a * f(\alpha, \Phi - \varepsilon_0), \qquad (6)$$

where C_0 is an unknown constant denoted by $\ln M_0/TE - R_2^i$, and ε_0 is an angle offset.[20] Throughout the WM across the whole brain, M_0 varied minimally as reported previously,[33] and thus was considered constant.

WM voxels were first segmented from high-resolution anatomical T_1-weighted volumetric images, and the valid WM voxels were further masked by the thresholds of 0.5 < FA < 0.9 and 0.5 < MO < 1.0, ensuring each voxel was better represented by a prolate diffusion

tensor.[20] After pooling and binning data from these selected WM voxels across the whole brain, the orientation-dependent R_2 profiles, i.e., $\ln S_{b=0}/TE$, were established as previously demonstrated in the literature,[20,21] and the corresponding four model parameters, i.e., C_0, R_2^a, α, and ε_0, were extracted based on Equation 6 via a nonlinear least-squares curve fitting method.

3.2 | Previously published orientation-dependent R_2^* profiles at 3 T and 7 T

A free online tool (www.graphreader.com) was used to extract previously published R_2^* orientation dependence profiles from the WM of the whole human brain or its selected fiber tracts of healthy subjects at 3T and 7T. These extracted relaxation data were originally measured following ethical guidelines as stated in the original publications.

The first R_2^* profile of the whole brain WM at 3 T,[34] without the confounding flip angle (FA) effect, was derived from different R_2^* profiles measured with FA = 6°, 17°, 35° and 60° by a linear regression, as described in the literature.[35] This FA-independent R_2^* profile at 3T was averaged from six subjects (age 22-29, median age 25). The second R_2^* profile of the whole brain WM at 7T, also without the confounding FA effect, was extracted directly from Figure 7 (Session2, green) of the original paper.[35] This profile was measured from three healthy subjects (age 38.7 ± 4.2 years).

The third and fourth R_2^* profiles were derived from the corpus callosum (CC) at 3T and 7T, and the fifth and sixth R_2^* profiles were obtained from the cingulum (CG) at 3T and 7T.[36] For these previously reported R_2^* profiles from the conference abstract, no specific demographic information about subjects was provided; however, a recent related publication on partial datasets showed that five healthy participants were involved with an average age of 34 ± 6 years.[37]

It is worth mentioning that the orientation information underlying the orientation-dependent R_2^* profiles at 7T was derived from 3T DTI.[35,36] Furthermore, the orientation information used for describing all R_2^* profiles, except for the second, was determined from the angle between the B_0 direction and the direction of the first peak of the orientation distribution function (ODF), rather than the direction (Φ) of the principal diffusivity as usual. The previously reported ODF was calculated using the constrained spherical deconvolution scheme on multi-shell diffusion datasets.[38] For convenience, these ODF-based angles were still denoted by Φ in this work.

3.3 | Data analysis and error estimations

Orientation-dependent R_2 profiles (i.e., $\ln S_{b=0}/TE$ at 3T and 7T) were generated using custom Python scripts for data binning and sorting, following established literature procedures.[39] These profiles contained 18 data points covering orientation angles (Φ) from 2.5° to 87.5°, with an angular resolution (AR) of 5°. The profiles were further quantified using Equation 6 through an unweighted nonlinear least-squares fitting procedure, implemented via an Interactive Data Language (IDL 9.1, Harris Geospatial Solutions, Inc., Broomfield, CO, USA) programming script from the public domain (http://purl.com/net/mpfit). The fitting function in Equation 6 included four model parameters constrained to the following ranges: C_0 = [0, 200] (1/s) and R_2^a = [0, 10] (1/s) for spin-echo based profiles; R_2^i = [0, 100] (1/s) and R_2^a = [0, 100] (1/s) for gradient-echo based profiles; α = [0°, 90°], and ε_0= [0°, 45°] for all profiles. Uncertainties for the fits were adjusted to achieve a reduced χ^2 of unity. Unless stated otherwise, standard deviations of the presented data were indicated by error bars or the half-widths of shaded ribbons. The MRtrix3 viewer (MRView) was used to visualize image data (Figure 2).[40]

4 | RESULTS

4.1 | Anisotropic R_2^a derived from spin-echo signals at 3T and 7T

Figure 3 compares the representative orientation (Φ) dependence profiles of anisotropic $R_2^a(\alpha, \Phi)$ between 3T (blue) and 7T (red) from Subject 15 (HCP_ID: 385046_M28). These profiles were derived from *b*-value (s/mm^2) of 1000 (Figure 3A) and 2000 (Figure 3B). For the former, the fitted R_2^a increased from 3.33 ± 0.33 (1/s) at 3T to 6.06 ± 0.63 (1/s) at 7T, while other fits such as α and ε_0 appeared to be comparable. The ratio η of R_2^a values between 7T and 3T was 1.82 ± 0.26. For the latter, this ratio (η = 2.08 ± 0.41) was almost the same within the measurement errors. These measured η values are far less than the theoretical ratio (η = 5.81) if the susceptibility effect was solely responsible for the observed orientation-dependent transverse relaxation in WM.

For all 25 subjects considered in this study, the fitted R_2^a values at 3T are plotted against those measured at 7T in Figure 4 for datasets with *b*-values (s/mm^2) of 1000 (Figure 4A) and 2000 (Figure 4C). In these plots, colored dashed lines illustrate the two theoretically predicted η values, corresponding to the two exclusive relaxation mechanisms: the susceptibility effect (η = 5.81, red) and MAE (η = 1.0, blue). The corresponding subject-specific η values are plotted in Figure 4B and Figure 4D, with an average around 1.5, as indicated by a dashed horizontal line. Details about the fitted parameters can be found in Table 1 for *b*-value=1000 (s/mm^2) and Table 2 for *b*-value=2000 (s/mm^2).

From 3T to 7T, as shown in Table 1, the fitted R_2^a values (1/s) increased, on average, from 3.6 ± 1.1 (1/s) to 5.4 ± 1.5 (1/s), or by ΔR_2^a = 1.8 ± 1.9 (1/s). A partial contribution from the susceptibility effect to the measured R_2^a at 3T can be estimated as $\Delta R_2^a/\eta$ = 0.31 ± 0.33 (1/s). In other words, MAE was essentially responsible for the measured R_2^a at 3T, with less than 10%

contribution from the susceptibility effect. The fitted α changed from 65.5 ± 3.1 (°) to 69.5 ± 1.7 (°), and the fitted ε_0 varied from 26.2 ± 3.8 (°) to 11.2 ± 11.3 (°). These fitted model parameters, and the corresponding changes, are consistent with those found in Table 2.

4.2 | Anisotropic R_2^a derived from gradient-echo signals at 3T and 7T

When comparing the fitted parameters from the orientation-dependent T_2^* profiles of the whole brain WM at 3T (Figure 5A) and 7T (Figure 5B), we found that the measured R_2^a values at the two magnetic fields are comparable within the precision limits, specifically 6.88 ± 0.32 (1/s) versus 7.05 ± 1.26 (1/s). Furthermore, no significant differences were found at 3T (blue) and 7T (red) in a different study from the literature,[36] when these derived R_2^a values were compared from specific fiber tracts, such as the corpus callosum (CC) in Figure 5C (10.98 ± 0.74 vs. 9.42 ± 2.91) and the cingulum (CG) in Figure 5D (11.03 ± 1.96 vs. 10.22 ± 2.05). These findings suggest that the susceptibility effect is not the primary anisotropic relaxation mechanism as previously thought,[13,14,16] which is consistent with the conclusion mentioned above.

5 | DISCUSSION

The aim of this study is to shed light on the long-standing puzzle concerning the origins of orientation-dependent transverse relaxation in human brain WM. By comparing anisotropic transverse relaxation rates at two different magnetic B_0 fields, we were able to distinguish the contributions from MAE and the susceptibility mechanism, thanks to their unique B_0 dependences. The findings from this study have significant implications for improving our understanding of anisotropic relaxation contrasts in MR imaging, thereby enhancing our insights into the microstructural organization of human brain WM

5.1 | B_0-dependent R_2^a from spin-echo signals

It has been well documented that the reported R_2^a in human brain WM depends not only on relaxation (e.g., spin-echo vs. gradient-echo) and diffusion (e.g., different b-values) data acquisition schemes but also on image post-processing methods (e.g., different WM voxel masks). Based on spin-echo signals (i.e., b-value = 0) from DTI datasets, we measured an average increase in R_2^a from 3T and 7T. We found that the previously proposed susceptibility effect contributed less than 10% to the measured R_2^a at 3T, indicating that MAE is the predominantly governing relaxation mechanism. This conclusion is consistent with our prior findings from reported B_0-dependent $T_{1\rho}$ dispersion datasets of rat brain WM in vivo.[21,41] Specifically, the susceptibility effect, which is equivalent to the chemical exchange effect in terms of the B_0^2-dependence, was found to be responsible for only 12.1% of the "dispersed" transverse relaxation rate at 3T.[21] This dispersed relaxation rate comprised contributions from both MAE and the susceptibility effect.

To our knowledge, this is the first characterization of orientation-dependent R_2 profiles based on spin-echo signals of human brain WM in vivo at 7T. Previously, such anisotropic R_2 profiles, based on standard R_2 mapping from formalin-fixed brain samples, were investigated using a 7T whole-body MRI scanner.[13] Interestingly, the observed orientation dependence in R_2 was insignificant compared to that in R_2^*. This unexpected observation led to the conclusion that the susceptibility effect was the primary origin of the observed anisotropic transverse relaxation in WM, although the investigators remained unclear to what extent MAE might have contributed to the underlying contrasts. This is mainly because MAE, rather than the susceptibility effect, could explain the temperature-dependent transverse relaxation anisotropies measured in the same study.

It is well acknowledged that human brain R_2 mapping using a 7 T whole-body MRI scanner is challenging,[30] primarily due to the relatively higher inhomogeneities in magnetic B_0 and B_1 fields and the more stringent SAR (specific absorption rate) controls or RF heating limitations. As a result, the profile of an imaging slice defined by both excitation 90° and multiple refocusing 180° RF pulses could be compromised in conventional R_2 mapping at 7T, potentially resulting in a biased relaxation metric, which in turn translates into a controversial anisotropic relaxation mechanism, as previously proposed and widely reported in the literature.[13,22]

Great effort has been made to mitigate the above mentioned limitations at 7T, making the acquisition of high-resolution whole-brain diffusion images feasible.[42] For diffusion data acquisition, a single refocusing 180° RF pulse is generally employed, thus lifting the SAR constraints to some degree compared to standard R_2 mapping. Since our interest rests on the anisotropic component of R_2, it is sufficient to collect R_2-weighted images with only one TE, as demonstrated in this study, if orientation information is available. This simple approach has been exploited in the literature for studying human knee articular cartilage in vivo[43] and animal cartilage samples ex vivo,[44] where the orientation information for the former came from intrinsic femoral bone geometry and for the latter from directly measuring samples rotations.

5.2 | B_0-dependent R_2^a from gradient-echo signals

Despite differences in data acquisition and analysis methods between the two separate investigations from different research groups,[34,35] the R_2^a values derived based on gradient-echo signals of whole brain WM remain compatible at both 3T (Figure 5A) and 7T (Figure 5B). For instance, the orientation of the axon fiber bundle within an image voxel was determined by the principal diffusion direction at 7T, whereas it was determined by the first peak direction of the

ODF at 3T. Furthermore, the WM mask for the orientation-dependent R_2^a profile at 7T was based on high-resolution structural T_1-weighted 3D images and further refined by an FA cutoff value (i.e., FA > 0.6). In contrast, no additional post-processing was performed on the WM mask derived from the first peak of the ODF at 3T.

When focusing on specific fiber tracts at the two magnetic fields, the derived R_2^a values (~10 1/s) from the same research group are still statistically indistinguishable,[36] albeit exhibiting an increase compared with those (~7 1/s) from the whole brain WM, as shown in Figure 5A and Figure 5B. These increases are primarily attributed to relatively higher microstructural anisotropies in the corpus callosum (Figure 5C) the cingulum (Figure 5D). It is worth noting that AR and the number of points (NP) of the measured orientation-dependent R_2^* profiles in Figure 5C (AR = 10°, NP = 7) and Figure 5D (AR = 10°, NP = 8) were much lower than those used in Figure 5A (AR = 5°, NP = 18) and Figure 5B (AR < 2°, NP = 44). These unfavorable AR and NP numbers may have contributed to the biased fits with relatively larger uncertainties reported in Figure 5C (e.g., α = 47.1 ± 8.3° at 7T) and Figure 5D (e.g., ε_0 = 18.9 ± 6.4° at 3T).

5.3 | Understanding MAE in biological tissues

Rotationally restricted water molecules are ubiquitous in biological tissues, and their unique magnetic relaxation characteristics can manifest orientation dependence relative to the direction of the B_0 field.[2] This phenomenon, known as MAE, is observed in tissues with highly organized microstructures, such as articular cartilage containing structured triple helix bundles[17] and brain WM containing ordered axon fibers.[20,21] In the literature, this orientation-dependent feature in transverse relaxation is typically characterized by the function $(3\cos^2\theta - 1)^2$, which becomes zero when the orientation angle θ is 54.7°.

It is crucial to understand that this standard orientation-dependent function $(3\cos^2\theta - 1)^2$ applies only to an ensemble of restricted water molecules with the same orientation.[18] Otherwise, an expansion or average of this function must be carried out according to the specific distribution of the restricted waters within a system,[45] resulting in dramatically different orientation dependence. In the literature,[18,45] this function expansion was performed for an axially symmetric distribution or a "cone" model and was recently reformatted as expressed in Equation 3.

When investigating MAE in human brain WM in the past, some researchers overlooked the fact that rotationally restricted water molecules do not align uniformly within the myelin sheath around an axon fiber.[13,16,27] Consequently, the measured R_2 or R_2^* was seemingly unexpectedly larger with an axon fiber perpendicular to B_0 than with an axon fiber parallel to B_0. This result appeared contradictory to the standard orientation-dependent function $(3\cos^2\theta - 1)^2$ and thus ruled out the possibility of MAE as an effective anisotropic relaxation mechanism in WM. Furthermore, the absence of cartilage within human brain parenchyma was used as a justification for not considering MAE.[19] It is the rotationally restricted water molecules, not their host molecules, that play a key role in defining how the measured R_2 or R_2^* depends on the orientation with respect to the direction of B_0.

When comparing MAE in the peripheral nervous system (PNS)[46,47] and in the central nervous system (CNS), researchers could have had difficulty explaining seemingly contradictory experimental results if Equation 3 had not been considered for the systems under investigation. Unlike the CNS, the PNS has extensive connective tissues composed primarily of collagen.[47,48] MAE arising from the restricted waters in collagen overshadows that from the restricted waters

within the myelin sheath.[48] Therefore, it seems that the PNS behaves normally following the standard MAE,[46] like tendons, while the CNS does not.[20,21]

Our discussions primarily focused on rotationally restricted water molecules in biological tissues. When we discuss a system of restricted waters, we are referring to an ensemble of vectors of residual dipolar interactions, with each vector connecting two protons within a water molecule. The residual dipolar interaction can arise from any pair of protons in tissues, such as methylene protons from alkyl chains of phospholipid in myelin.[21,49] Without loss of generalization, we can say that MAE occurs ubiquitously in highly organized biological tissues, and the human brain WM is no exception.

5.4 | Understanding the susceptibility effect in biological tissues

When the susceptibility effect was proposed as the origin for anisotropic transverse relaxation contrasts in human brain WM, the primary focus was on better characterizing the shape of the R_2 or R_2^* profile.[13,14,16] However, a key question was overlooked: whether the strength of the proposed effect is sufficient to explain the observed R_2 or R_2^* anisotropy. In the literature,[50] this aspect has been discussed regarding the observed R_1 anisotropy in human brain WM.

The susceptibility anisotropy of the myelin sheath, defined by the susceptibility difference of an axon fiber orientated perpendicular versus parallel to B_0, was reported to be approximately 0.012 ppm at 7T.[51] This measured susceptibility anisotropy translates into a chemical shift difference $\Delta\omega$ of approximately 1.533*2π (rad/s) at 3T. Accordingly, its square $(\Delta\omega)^2$ will become 92.78 (rad/s)^2. When evaluating the theoretical contribution of the measured susceptibility anisotropy in terms of the chemical exchange effect, this predicted value, calculated by $(\Delta\omega)^2 * \tau_{chex}$, would be 0.093 (rad/s) or simply 0.093 (1/s), assuming an exchange timescale (τ_{chex}) of 1 (ms/rad) or simply 1 (ms). This rough estimation is performed without

considering the molecular fractions (i.e., f_A and f_B) between two fast-exchanging states. As typically discussed in the literature,[29] an appropriate function should be given by $f_A * f_B * (\Delta\omega)^2 * \tau_{chex}$, with a maximum $f_A * f_B$ of 0.25.

Considering that the measured R_2^a at 3T from this work was generally larger than 3.6 (1/s), we can reasonably conclude that the previously proposed susceptibility effect is insufficient to explain the observed R_2^a in human brain WM. In the past, the susceptibility effect has also been theoretically demonstrated to be an insignificant pathway for anisotropic longitudinal R_1 relaxation in WM.[50] It is worth mentioning that the timescales of water tumbling responsible for R_1 relaxation are between picoseconds and nanoseconds. These "fast" molecular motions are only active on orientation-independent transverse relaxation, while "slow" molecular motions, with the timescales between microsecond and milliseconds, are responsible for the observed R_2^a.[28,52]

When considering partially ordered waters engaging in fast-exchange processes with bulk free water molecules in biological tissues, the above mentioned $\Delta\omega$ can theoretically range from zero to approximately 30 kHz[52] – the strength of the dipolar interaction between two protons separated by 1.59Å in a rigid water molecule.[18] Therefore, unlike the susceptibility effect, MAE has a solid physical basis as a dominant anisotropic transverse relaxation mechanism in highly organized biological tissues in general, and in human brain WM specifically.

6 | CONCLUSIONS

This study suggests that MAE is the primary orientation-dependent transverse relaxation mechanism at 3T in human brain WM, offering a different perspective from previous literature. Our conclusion is supported by experimental findings at two magnetic fields from both spin-echo

and gradient-echo signals. The observed MAE in highly organized biological tissues should be evaluated for an ensemble of rotationally restricted water molecules distributed differently within the system under investigation, and the human brain WM is no exception.

DATA AVAILABILITY STATEMENT

Data and Python/IDL scripts used in this work are available upon request from the authors.

CONFLICT OF INTEREST

The author has no conflicts of interest to declare.

FUNDING INFORMATION

This work was partially funded by the American Lebanese Syrian Associated Charities (ALSAC) at St. Jude Children's Research Hospital.

ORCID

Yuxi Pang: https://orcid.org/0000-0001-5039-0236

Wilburn E. Reddick: https://orcid.org/0000-0002-1054-1201

REFERENCES

1. Gore JC, Kennan RP. Physical and physiological basis of magnetic relaxation. *Magn Reson Imaging*. 1999;1:33-42.
2. Mathur-De Vre R. The NMR studies of water in biological systems. *Progress in Biophysics and Molecular Biology*. 1980;35:103-134.
3. Duyn JH, van Gelderen P, Li T-Q, de Zwart JA, Koretsky AP, Fukunaga M. High-field MRI of brain cortical substructure based on signal phase. *Proceedings of the National Academy of Sciences*. 2007;104(28):11796-11801.
4. Li T-Q, van Gelderen P, Merkle H, Talagala L, Koretsky AP, Duyn J. Extensive heterogeneity in white matter intensity in high-resolution T2*-weighted MRI of the human brain at 7.0 T. *Neuroimage*. 2006;32(3):1032-1040.
5. Wiggins C, Gudmundsdottir V, Le Bihan D, Lebon V, Chaumeil M. Orientation dependence of white matter T2* contrast at 7T: a direct demonstration. In: Proceedings of the International Society of Magnetic Resonance Medicine, Toronto, Canada, 2008. (abstract: 237):
6. Cherubini A, Péran P, Hagberg GE, et al. Characterization of white matter fiber bundles with T2* relaxometry and diffusion tensor imaging. *Magn Reson Med*. 2009;61(5):1066-1072.
7. Bender B, Klose U. The in vivo influence of white matter fiber orientation towards B0 on T2* in the human brain. *NMR Biomed*. 2010;23(9):1071-1076.
8. Denk C, Torres EH, MacKay A, Rauscher A. The influence of white matter fibre orientation on MR signal phase and decay. *NMR Biomed*. 2011;24(3):246-252.
9. Lee J, van Gelderen P, Kuo L-W, Merkle H, Silva AC, Duyn JH. T2*-based fiber orientation mapping. *Neuroimage*. 2011;57(1):225-234.
10. Bartels LM, Doucette J, Birkl C, Zhang Y, Weber AM, Rauscher A. Orientation dependence of R2 relaxation in the newborn brain. *NeuroImage*. 2022;264:119702.
11. Lenz C, Berger C, Bauer M, Scheurer E, Birkl C. Sensitivity of fiber orientation dependent R2∗ to temperature and post mortem interval. *Magn Reson Med*. 2021;86(5):2703-2715.
12. Birkl C, Doucette J, Fan M, Hernandez-Torres E, Rauscher A. Myelin water imaging depends on white matter fiber orientation in the human brain. *Magn Reson Med*. 2021;85(4):2221-2231.
13. Oh S-H, Kim Y-B, Cho Z-H, Lee J. Origin of B0 orientation dependent R2*(= 1/T2*) in white matter. *Neuroimage*. 2013;73:71-79.
14. Wharton S, Bowtell R. Gradient echo based fiber orientation mapping using R2* and frequency difference measurements. *Neuroimage*. 2013;83:1011-1023.
15. Wharton S, Bowtell R. Fiber orientation-dependent white matter contrast in gradient echo MRI. *Proc Natl Acad Sci USA*. 2012;109(45):18559-18564.
16. Knight MJ, Dillon S, Jarutyte L, Kauppinen RA. Magnetic resonance relaxation anisotropy: Physical principles and uses in microstructure imaging. *Biophys J*. 2017;112(7):1517-1528.
17. Bydder M, Rahal A, Fullerton GD, Bydder GM. The magic angle effect: a source of artifact, determinant of image contrast, and technique for imaging. *J Magn Reson Imaging*. 2007;25(2):290-300.

18. Berendsen HJC. Nuclear magnetic resonance study of collagen hydration. *J Chem Phys*. 1962;36(12):3297-3305.
19. Knight MJ, Wood B, Couthard E, Kauppinen R. Anisotropy of spin-echo T2 relaxation by magnetic resonance imaging in the human brain in vivo. *Biomed Spectrosc Imaging*. 2015;4(3):299-310.
20. Pang Y. Phase shifted transverse relaxation orientation dependences in human brain white matter. *NMR Biomed*. 2023;10.1002/nbm.4925doi:10.1002/nbm.4925
21. Pang Y. Orientation dependent proton transverse relaxation in human brain white matter: The magic angle effect on a cylindrical helix. *Magnetic Resonance Imaging*. 2023;100:73-83.
22. Tax CMW, Kleban E, Chamberland M, Baraković M, Rudrapatna U, Jones DK. Measuring compartmental T(2)-orientational dependence in human brain white matter using a tiltable RF coil and diffusion-T(2) correlation MRI. *Neuroimage*. 2021;236:117967.
23. Gil R, Khabipova D, Zwiers M, Hilbert T, Kober T, Marques JP. An in vivo study of the orientation‐dependent and independent components of transverse relaxation rates in white matter. *NMR Biomed*. 2016;29(12):1780-1790.
24. Yablonskiy DA, Haacke EM. Theory of NMR signal behavior in magnetically inhomogeneous tissues: the static dephasing regime. *Magn Reson Med*. 1994;32(6):749-763.
25. Simons M, Nave K-A. Oligodendrocytes: myelination and axonal support. *Cold Spring Harbor perspectives in biology*. 2016;8(1):a020479.
26. Beaulieu C. The biological basis of diffusion anisotropy. *Diffusion MRI*. Elsevier; 2014:155-183.
27. Cheng J-X, Pautot S, Weitz DA, Xie XS. Ordering of water molecules between phospholipid bilayers visualized by coherent anti-Stokes Raman scattering microscopy. *Proc Natl Acad Sci USA*. 2003;100(17):9826-9830.
28. Pang Y. An order parameter without magic angle effect (OPTIMA) derived from R1ρ dispersion in ordered tissue. *Magn Reson Med*. 2020;83(5):1783-1795.
29. Mlynarik V, Szomolanyi P, Toffanin R, Vittur F, Trattnig S. Transverse relaxation mechanisms in articular cartilage. *J Magn Reson*. Aug 2004;169(2):300-307. doi:10.1016/j.jmr.2004.05.003
30. van Gelderen P, Wang Y, de Zwart JA, Duyn JH. Dependence of brain-tissue R(2) on MRI field strength. *Magn Reson Med*. May 2025;93(5):2140-2152. doi:10.1002/mrm.30400
31. Smith SM, Jenkinson M, Woolrich MW, et al. Advances in functional and structural MR image analysis and implementation as FSL. *Neuroimage*. 2004;23:S208-S219.
32. Ennis DB, Kindlmann G. Orthogonal tensor invariants and the analysis of diffusion tensor magnetic resonance images. *Magn Reson Med*. 2006;55(1):136-146.
33. Schyboll F, Jaekel U, Weber B, Neeb H. The impact of fibre orientation on T 1-relaxation and apparent tissue water content in white matter. *MAGMA*. 2018;31(4):501-510.
34. Sibgatulin R, Deistung A, Güllmar D, Birkl C, Ropele S, Reichenbach JR. In vivo assessment of the anisotropy of R2* maps in white matter. In: Proceedings of the International Society of Magnetic Resonance Medicine, Montreal, CA 2019. (abstract: 4906):
35. Milotta G, Corbin N, Lambert C, Lutti A, Mohammadi S, Callaghan MF. Mitigating the impact of flip angle and orientation dependence in single compartment R2* estimates via 2‐pool modeling. *Magn Reson Med*. 2023;89(1):128-143.
36. Chen L, Mao D, Gilbert G, Versluis M, van Zijl P, Li X. Orientation dependence of local frequency difference and R2* in parallel versus crossing fibers at 3T and 7T. In: Proceedings of the International Society of Magnetic Resonance Medicine, London, UK, 2022. (abstract: 1643):

37. Chen L, Shin HG, van Zijl PCM, Li X. Exploiting gradient-echo frequency evolution: Probing white matter microstructure and extracting bulk susceptibility-induced frequency for quantitative susceptibility mapping. *Magn Reson Med*. Apr 2024;91(4):1676-1693. doi:10.1002/mrm.29958
38. Tournier JD, Calamante F, Connelly A. Robust determination of the fibre orientation distribution in diffusion MRI: non-negativity constrained super-resolved spherical deconvolution. *Neuroimage*. May 1 2007;35(4):1459-72. doi:10.1016/j.neuroimage.2007.02.016
39. Hernández-Torres E, Wiggermann V, Hametner S, et al. Orientation dependent MR signal decay differentiates between people with MS, their asymptomatic siblings and unrelated healthy controls. *Plos One*. 2015;10(10):e0140956.
40. Tournier JD, Smith R, Raffelt D, et al. MRtrix3: A fast, flexible and open software framework for medical image processing and visualisation. *Neuroimage*. Nov 15 2019;202:116137. doi:10.1016/j.neuroimage.2019.116137
41. Mäkelä HI, De Vita E, Gröhn OH, et al. B0 dependence of the on‐resonance longitudinal relaxation time in the rotating frame (T1 ρ) in protein phantoms and rat brain in vivo. *Magn Reson Med*. 2004;51(1):4-8.
42. Vu AT, Auerbach E, Lenglet C, et al. High resolution whole brain diffusion imaging at 7T for the Human Connectome Project. *Neuroimage*. Nov 15 2015;122:318-31. doi:10.1016/j.neuroimage.2015.08.004
43. Pang Y, Palmieri-Smith RM, Malyarenko DI, Swanson SD, Chenevert TL. A unique anisotropic R2 of collagen degeneration (ARCADE) mapping as an efficient alternative to composite relaxation metric (R2 -R1 rho) in human knee cartilage study. *Magn Reson Med*. 2019;81(6):3763-3774.
44. Grunder W. MRI assessment of cartilage ultrastructure. *NMR Biomed*. 2006;19(7):855-876.
45. Pang Y. Characterization of anisotropic T2W signals from human knee femoral cartilage: The magic angle effect on a spherical surface. *NMR Biomed*. 2021;34(7):e4535.
46. Chappell KE, Robson MD, Stonebridge-Foster A, et al. Magic angle effects in MR neurography. *AJNR Am J Neuroradiol*. Mar 2004;25(3):431-40.
47. Kästel T, Heiland S, Bäumer P, Bartsch A, Bendszus M, Pham M. Magic angle effect: a relevant artifact in MR neurography at 3T? *AJNR Am J Neuroradiol*. 2011;32(5):821-827.
48. Shinar H, Eliav U, Navon G. Deuterium double quantum-filtered NMR studies of peripheral and optic nerves. *MAGMA*. Dec 2021;34(6):889-902. doi:10.1007/s10334-021-00949-6
49. Pampel A, Müller DK, Anwander A, Marschner H, Möller HE. Orientation dependence of magnetization transfer parameters in human white matter. *Neuroimage*. 2015;114:136-146.
50. Schyboll F, Jaekel U, Petruccione F, Neeb H. Origin of orientation‐dependent R1 (= 1/T1) relaxation in white matter. *Magnet Reson Med*. 2020;84(5):2713-2723.
51. Lee J, Shmueli K, Fukunaga M, et al. Sensitivity of MRI resonance frequency to the orientation of brain tissue microstructure. *Proceedings of the National Academy of Sciences*. 2010;107(11):5130-5135.
52. Momot KI, Pope JM, Wellard RM. Anisotropy of spin relaxation of water protons in cartilage and tendon. *NMR Biomed*. 2010;23(3):313-24.

FIVE FIGURES

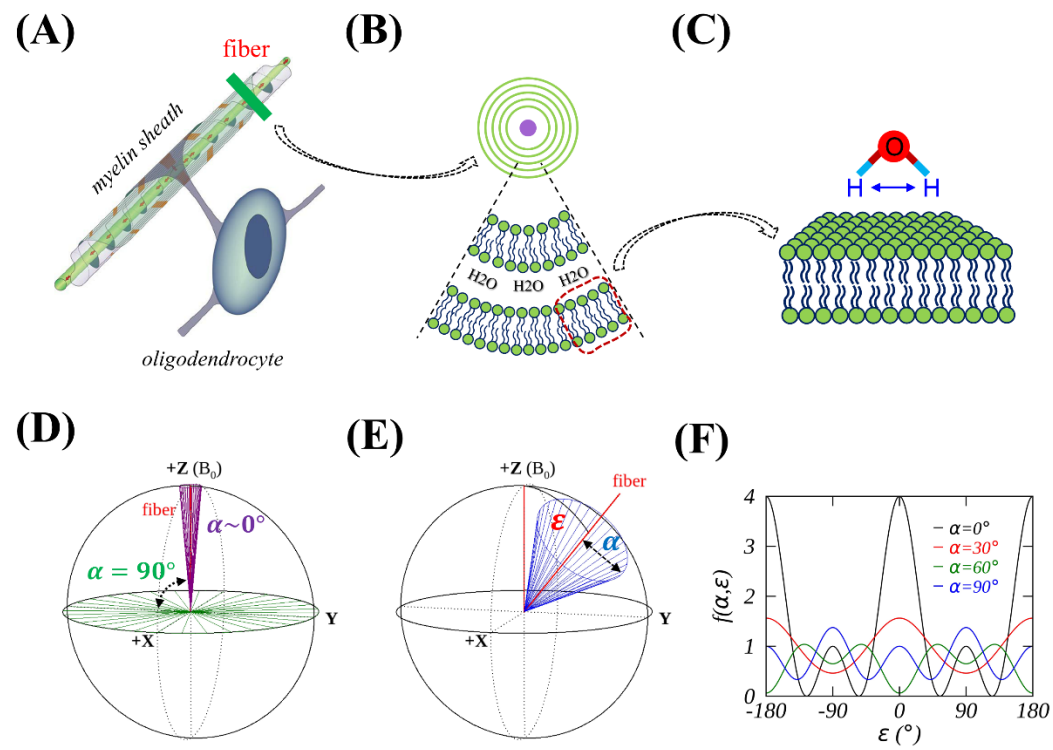

FIGURE 1. *Schematics of hierarchical structures of rotationally restricted waters from an axon fiber and a cone model for orientation-dependent transverse relaxation. (A) Myelinated axon fiber, adapted from Reference 25. (B) Plane perpendicular to the fiber showing restricted waters residing within (filled violet circle) and outside (sandwiched between membrane bilayers) the axon fiber. (C) Restricted waters in proximity to the membrane surface. (D) Restricted waters within the axon fiber (α = 0°, violet) and outside (α = 90°, green) the axon fiber. (E) Cone model with an open angle α, orientated at an angle ε to* B_0*. (F) Theoretical orientation dependences of transverse relaxation. Note: when referencing the orientation of restricted water, this refers to the direction of residual dipolar interaction between two protons within the water, as schematically shown in (C).*

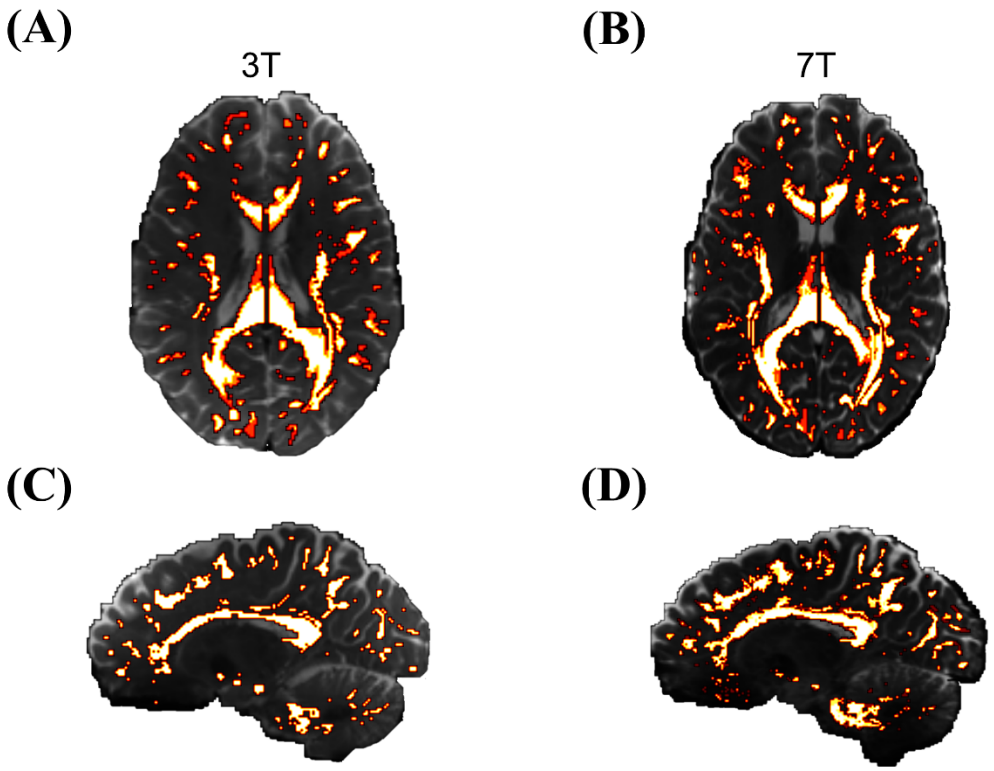

FIGURE 2. *White matter masks superimposed on T_2-weighted (b-value = 0) axial (A, B) and sagittal (C, D) images from 3T (A, C) and 7T (B, D) DTI datasets.*

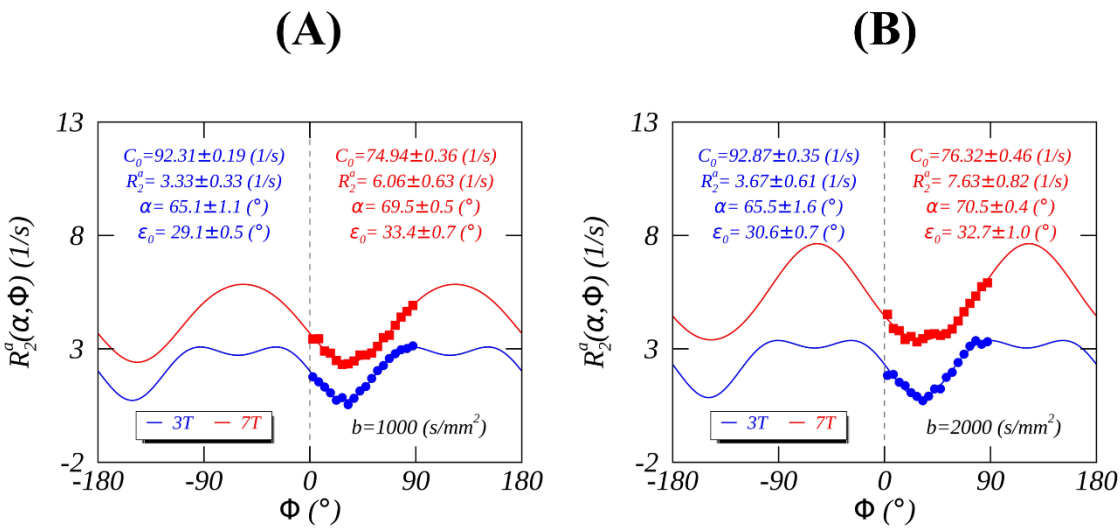

FIGURE 3. *Measured (colored symbols) and fitted (colored lines) orientation-dependent transverse relaxation rates $R_2^a(\alpha,\Phi)$ from Subject 15 at 3T (blue) and 7T (red), based on DTI using non-zero b-values (s/mm²) of 1000 (A) and 2000 (B).*

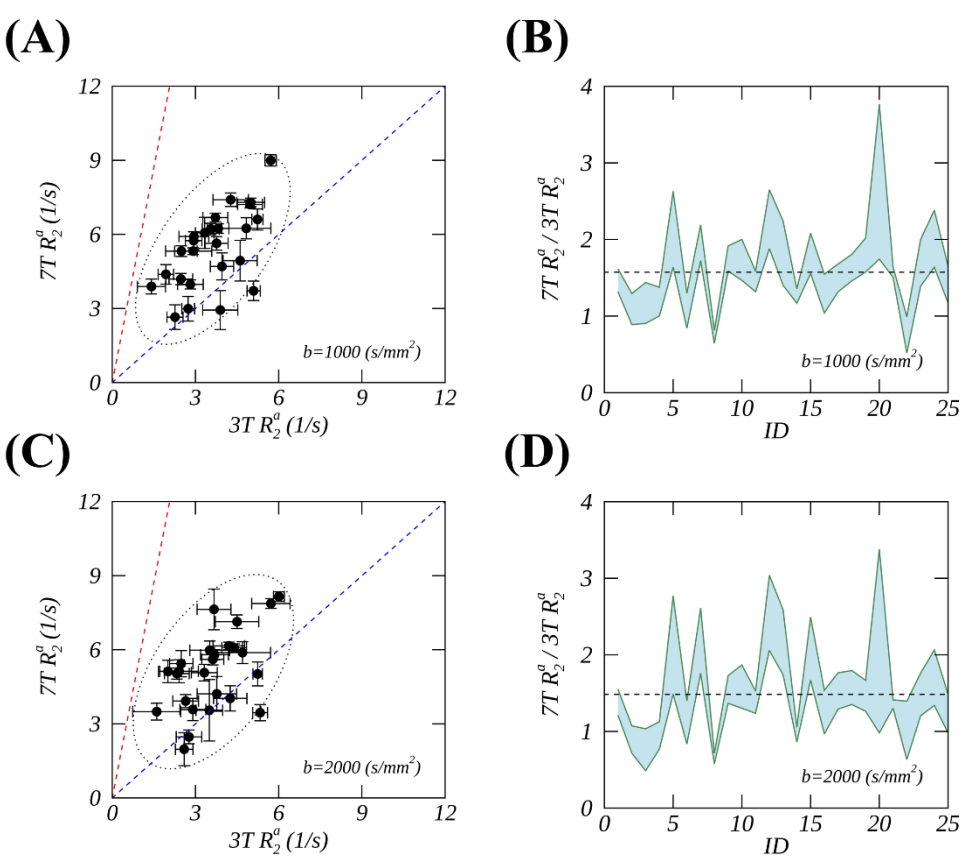

FIGURE 4. *Scatterplots (A, C) and ratio plots (B, D) of derived R_2^a from 7T and 3T DTI datasets on 25 subjects. DTI datasets were obtained using non-zero b-values (s/mm^2) of 1000 (A, B) and 2000 (C, D). The colored dashed lines represent the theoretical ratios of $R_2^a(7T)/R_2^a(3T)$ when the anisotropic transverse relaxation mechanism is due to the susceptibility effect (red) and the magic angle effect (blue). The horizontal dashed lines denote average ratios of $R_2^a(7T)/R_2^a(3T)$ from 25 subjects.*

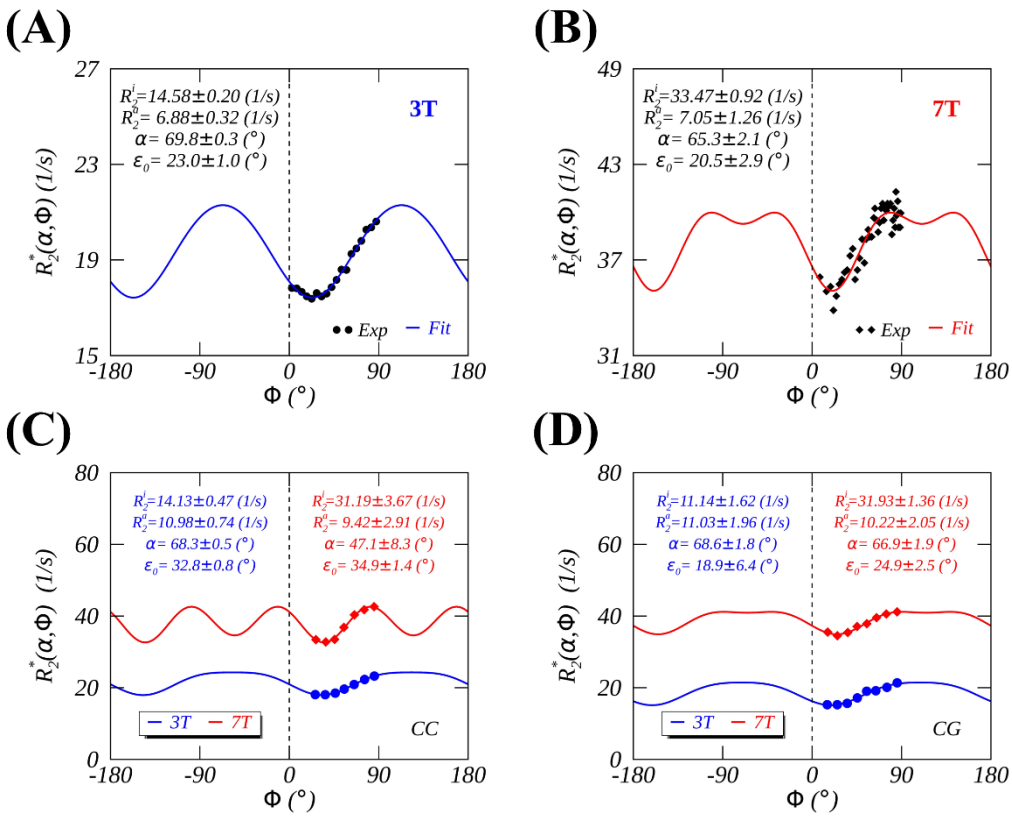

FIGURE 5. *Measured (colored symbols) and fitted (colored lines) orientation-dependent transverse relaxation rates $R_2^*(\alpha,\Phi)$ at 3T (blue lines) and 7T (red lines). Orientation-dependent R_2^* profiles were derived from: (A, B) whole brain WM; (C) corpus callosum; (D) cingulum.*

TWO TABLES

TABLE 1. Fitted four model parameters for an orientation-dependent transverse relaxation model for 25 subjects based on DTI datasets using a non-zero b-value of 1000 (s/mm²) at 3T and 7T. Data are shown as mean ± standard deviation.

Number	HCP_ID	3T (*b*=1000 s/mm²)				7T (*b*=1000 s/mm²)			
		C_0 (1/s)	R_2^a (1/s)	α (°)	ε_0 (°)	C_0 (1/s)	R_2^a (1/s)	α (°)	ε_0 (°)
1	100610_M28	93.9 ± 0.3	5.0 ± 0.5	67.8 ± 0.8	25.9 ± 1.0	79.6 ± 0.1	7.3 ± 0.2	68.4 ± 0.2	20.0 ± 0.5
2	126426_F33	91.8 ± 0.1	2.7 ± 0.2	67.3 ± 0.7	28.6 ± 0.6	77.0 ± 0.6	3.0 ± 0.5	69.0 ± 2.0	0.3 ± 14.3
3	130114_M28	92.3 ± 0.1	2.3 ± 0.3	58.7 ± 3.3	26.4 ± 0.7	76.5 ± 0.3	2.6 ± 0.5	67.4 ± 1.7	22.8 ± 2.2
4	130518_F33	92.7 ± 0.2	4.0 ± 0.4	65.5 ± 1.1	26.0 ± 0.7	78.2 ± 0.4	4.7 ± 0.5	67.9 ± 1.1	17.8 ± 2.4
5	134627_M28	92.9 ± 0.3	2.5 ± 0.6	62.6 ± 3.2	32.2 ± 0.7	77.5 ± 0.2	5.3 ± 0.2	69.7 ± 0.5	12.3 ± 3.0
6	135124_F33	93.0 ± 0.4	4.6 ± 0.6	67.6 ± 1.0	28.1 ± 1.0	78.4 ± 0.5	4.9 ± 0.8	70.9 ± 3.0	5.7 ± 25.1
7	146735_F33	92.2 ± 0.2	2.9 ± 0.3	67.5 ± 0.8	27.4 ± 0.8	79.0 ± 0.2	5.7 ± 0.4	70.8 ± 0.4	23.4 ± 1.9
8	148133_F28	93.0 ± 0.1	5.1 ± 0.2	68.3 ± 0.3	26.6 ± 0.5	77.2 ± 0.3	3.7 ± 0.4	67.7 ± 1.0	20.9 ± 1.6
9	165436_M28	93.6 ± 0.2	3.5 ± 0.3	66.0 ± 0.9	23.7 ± 0.7	79.8 ± 0.2	6.2 ± 0.2	70.4 ± 0.3	0.0 ± 0.0
10	167440_F28	92.0 ± 0.4	4.3 ± 0.6	67.8 ± 1.2	25.1 ± 1.5	81.5 ± 0.2	7.4 ± 0.3	70.2 ± 0.3	0.0 ± 0.0
11	177140_F33	95.3 ± 0.3	5.0 ± 0.4	67.5 ± 0.8	23.9 ± 1.0	82.5 ± 0.1	7.2 ± 0.1	71.8 ± 0.2	0.0 ± 0.0
12	180533_F33	92.1 ± 0.1	1.9 ± 0.3	58.3 ± 3.8	30.4 ± 0.6	77.9 ± 0.2	4.4 ± 0.4	67.0 ± 0.9	22.6 ± 1.0
13	193845_M28	92.2 ± 0.4	2.9 ± 0.7	62.4 ± 3.2	33.5 ± 0.6	78.3 ± 0.1	5.3 ± 0.1	71.4 ± 0.4	1.6 ± 2.7
14	360030_F33	94.3 ± 0.2	5.2 ± 0.2	68.9 ± 0.4	14.5 ± 1.5	78.3 ± 0.3	6.6 ± 0.4	69.4 ± 0.5	0.0 ± 0.0
15	385046_M28	92.3 ± 0.2	3.3 ± 0.3	65.1 ± 1.1	29.1 ± 0.5	74.9 ± 0.4	6.1 ± 0.6	69.5 ± 0.5	33.4 ± 0.7
16	401422_F33	94.2 ± 0.5	4.8 ± 0.9	68.7 ± 1.2	27.7 ± 1.8	80.6 ± 0.3	6.2 ± 0.4	70.1 ± 0.4	26.0 ± 1.2
17	463040_F33	92.6 ± 0.3	3.8 ± 0.4	67.2 ± 1.0	25.5 ± 1.0	79.0 ± 0.3	5.6 ± 0.3	70.8 ± 1.2	2.3 ± 9.9
18	644246_F33	93.5 ± 0.2	3.8 ± 0.4	67.5 ± 0.9	23.9 ± 1.1	80.0 ± 0.2	6.2 ± 0.2	68.6 ± 0.3	12.9 ± 1.2
19	654552_F33	93.6 ± 0.3	3.7 ± 0.4	66.3 ± 1.2	24.7 ± 1.0	79.7 ± 0.2	6.7 ± 0.2	69.7 ± 0.4	11.8 ± 2.0
20	757764_F36	90.8 ± 0.2	1.4 ± 0.5	58.1 ± 10.5	27.1 ± 2.0	77.3 ± 0.2	3.9 ± 0.3	71.8 ± 0.6	0.0 ± 0.0
21	765864_F28	95.6 ± 0.1	5.7 ± 0.2	68.0 ± 0.3	19.2 ± 0.7	82.6 ± 0.2	9.0 ± 0.2	71.4 ± 0.2	0.0 ± 0.0
22	878877_M28	92.3 ± 0.4	3.9 ± 0.6	65.5 ± 1.7	27.5 ± 1.0	71.8 ± 0.4	2.9 ± 0.8	64.5 ± 2.8	34.1 ± 0.8
23	905147_F36	92.0 ± 0.3	2.5 ± 0.4	65.9 ± 1.8	23.4 ± 1.5	77.1 ± 0.2	4.2 ± 0.2	69.1 ± 0.5	0.0 ± 0.0
24	943862_M28	93.3 ± 0.3	2.9 ± 0.5	65.4 ± 1.9	28.7 ± 0.9	79.3 ± 0.2	5.9 ± 0.2	68.0 ± 0.3	12.1 ± 1.1
25	971160_M28	93.4 ± 0.3	2.8 ± 0.5	64.0 ± 2.1	26.4 ± 0.9	78.2 ± 0.1	4.0 ± 0.2	71.8 ± 0.4	0.0 ± 0.0
mean ± std		93.0 ± 1.1	3.6 ± 1.1	65.5 ± 3.1	26.2 ± 3.8	78.5 ± 2.2	5.4 ± 1.5	69.5 ± 1.7	11.2 ± 11.3

TABLE 2. Fitted four model parameters for an orientation-dependent transverse relaxation model for 25 subjects based on DTI datasets using a non-zero b-value of 2000 (s/mm²) at 3T and 7T. Data are shown as mean ± standard deviation.

Number	HCP_ID	3T (b=2000 s/mm^2)				7T (b=2000 s/mm^2)			
		C_0 (1/s)	R_2^a (1/s)	α (°)	ε_0 (°)	C_0 (1/s)	R_2^a (1/s)	α (°)	ε_0 (°)
1	100610_M28	94.5 ± 0.4	5.7 ± 0.7	68.7 ± 0.8	27.2 ± 1.2	80.3 ± 0.1	7.9 ± 0.2	69.4 ± 0.2	21.6 ± 0.6
2	126426_F33	92.0 ± 0.3	2.8 ± 0.5	67.8 ± 1.2	29.8 ± 1.1	76.8 ± 0.2	2.5 ± 0.3	68.7 ± 0.9	0.0 ± 0.0
3	130114_M28	92.7 ± 0.2	2.6 ± 0.3	59.9 ± 2.6	28.6 ± 0.5	76.6 ± 0.4	2.0 ± 0.7	64.7 ± 3.5	33.8 ± 1.0
4	130518_F33	93.0 ± 0.4	4.3 ± 0.6	66.3 ± 1.3	26.9 ± 1.0	77.9 ± 0.3	4.0 ± 0.5	67.7 ± 1.2	19.4 ± 2.2
5	134627_M28	93.0 ± 0.3	2.4 ± 0.7	61.2 ± 4.7	34.2 ± 0.8	78.0 ± 0.1	5.1 ± 0.5	71.3 ± 1.0	7.4 ± 8.8
6	135124_F33	92.7 ± 0.4	3.8 ± 0.7	66.2 ± 1.7	29.3 ± 1.0	78.1 ± 0.6	4.2 ± 0.7	70.8 ± 3.7	4.1 ± 31.3
7	146735_F33	92.0 ± 0.2	2.5 ± 0.4	66.1 ± 1.5	30.3 ± 0.8	79.1 ± 0.2	5.4 ± 0.5	71.7 ± 0.5	17.9 ± 4.9
8	148133_F28	93.3 ± 0.2	5.3 ± 0.3	68.8 ± 0.3	26.6 ± 0.6	77.3 ± 0.2	3.5 ± 0.3	68.8 ± 0.8	19.9 ± 2.1
9	165436_M28	93.8 ± 0.2	3.6 ± 0.4	66.3 ± 1.1	25.1 ± 0.9	79.7 ± 0.2	5.6 ± 0.2	70.7 ± 0.3	0.0 ± 0.0
10	167440_F28	92.3 ± 0.5	4.5 ± 0.8	68.3 ± 1.3	26.1 ± 1.8	81.5 ± 0.2	7.1 ± 0.3	70.4 ± 0.3	0.0 ± 0.0
11	177140_F33	95.1 ± 0.3	4.4 ± 0.4	66.8 ± 0.9	25.2 ± 0.9	82.0 ± 0.1	6.1 ± 0.2	71.6 ± 0.2	0.0 ± 0.0
12	180533_F33	92.3 ± 0.2	2.0 ± 0.3	59.4 ± 3.8	31.5 ± 0.6	78.6 ± 0.3	5.1 ± 0.5	68.7 ± 0.7	22.4 ± 1.5
13	193845_M28	92.1 ± 0.2	2.3 ± 0.4	57.3 ± 5.8	35.0 ± 0.6	78.3 ± 0.1	5.0 ± 0.2	72.1 ± 0.4	3.2 ± 2.9
14	360030_F33	94.5 ± 0.1	5.2 ± 0.2	69.3 ± 0.4	14.6 ± 1.5	77.8 ± 0.4	5.0 ± 0.5	69.4 ± 0.8	0.0 ± 0.0
15	385046_M28	92.9 ± 0.3	3.7 ± 0.6	65.5 ± 1.6	30.6 ± 0.7	76.3 ± 0.5	7.6 ± 0.8	70.5 ± 0.4	32.7 ± 1.0
16	401422_F33	94.3 ± 0.6	4.7 ± 1.0	68.8 ± 1.3	28.6 ± 1.9	80.7 ± 0.3	5.9 ± 0.4	70.9 ± 0.4	25.1 ± 1.8
17	463040_F33	92.5 ± 0.3	3.3 ± 0.5	66.0 ± 1.3	27.5 ± 0.9	78.8 ± 0.3	5.1 ± 0.3	70.8 ± 1.5	0.8 ± 12.2
18	644246_F33	93.5 ± 0.3	3.7 ± 0.5	67.6 ± 1.1	25.3 ± 1.3	79.9 ± 0.2	5.8 ± 0.2	69.3 ± 0.5	10.0 ± 2.4
19	654552_F33	94.1 ± 0.3	4.2 ± 0.6	67.1 ± 1.1	27.2 ± 1.0	80.2 ± 0.1	6.2 ± 0.2	71.7 ± 0.2	0.0 ± 0.0
20	757764_F36	91.5 ± 1.0	1.6 ± 0.9	43.1 ± 6.2	29.7 ± 2.1	77.2 ± 0.3	3.5 ± 0.3	71.7 ± 0.8	0.0 ± 0.0
21	765864_F28	95.8 ± 0.1	6.0 ± 0.2	68.2 ± 0.3	20.3 ± 0.6	82.3 ± 0.1	8.2 ± 0.2	71.9 ± 0.2	0.0 ± 0.0
22	878877_M28	92.4 ± 0.3	3.5 ± 0.5	63.8 ± 1.7	30.5 ± 0.5	72.7 ± 0.7	3.5 ± 1.2	66.8 ± 2.6	35.2 ± 1.2
23	905147_F36	92.3 ± 0.3	2.6 ± 0.5	67.0 ± 1.6	24.9 ± 1.6	77.1 ± 0.2	3.9 ± 0.3	68.6 ± 0.6	0.0 ± 0.0
24	943862_M28	93.7 ± 0.4	3.5 ± 0.7	65.2 ± 2.0	32.7 ± 0.7	79.8 ± 0.3	6.0 ± 0.4	69.2 ± 0.7	13.6 ± 3.0
25	971160_M28	93.6 ± 0.3	2.9 ± 0.5	64.2 ± 2.0	27.9 ± 0.8	78.0 ± 0.2	3.6 ± 0.4	72.2 ± 1.1	4.3 ± 7.5
mean ± std		93.2 ± 1.1	3.6 ± 1.2	64.8 ± 5.4	27.8 ± 4.1	78.6 ± 2.0	5.1 ± 1.6	70.0 ± 1.8	10.9 ± 12.0